2024 IEEE International Conference on Robotics and Automation (ICRA 2024)
May 13-17, 2024. Yokohama, Japan

Design and Fabrication of a Novel Miniature Magnetic Gripper

Mengde Li[1,2], Fuqiang Zhao[3], Xiangli Li[1], Mingchang Li[4], Sheng Liu[1], *Senior Member, IEEE* and Miao Li[1,5,*], *Senior Member, IEEE*

***Abstract*— Small-scale robots hold significant promise in the field of minimally invasive surgery (MIS). In this paper, we present a miniature magnetic gripper and develop a data-driven kinematic model. The gripper comprises four fingers, wherein each finger has a maximum size not exceeding 3mm, 4mm and 5.5mm in three dimensions. By integrating permanent magnets and elastic ropes as internal actuation elements into the fingers, the gripper is equipped with the capability to open-close under an external magnetic field, facilitating the manipulation of small objects in confined spaces. Modeling and analysis of the magnetic gripper are undertaken, wherein the relationship between the open angle and the external magnetic field is established. The average error between the experimentally observed open angles and the model-predicted values is 2.31°. Subsequent experiments demonstrated the necessity of the magnetic gripper model for precise manipulation, verified its excellent sensitivity to magnetic fields, and demonstrated its potential for future applications in MIS.**

I. INTRODUCTION

Miniaturized robotic grippers have garnered significant attention due to their compact size and exceptional maneuverability in confined spaces [1], [2]. These merits have attracted widespread research interest across diverse fields, including micro-manipulation, micro-assembly, drug delivery and MIS. Multiple methods have been employed to actuate the miniature robots including light-driven, thermal-driven, ultrasonic-driven, chemical-driven, and magnetic-driven [3], [4]. Among these approaches, magnetic actuation emerging as an indirect yet reliable control method with substantial potential for remote manipulation. The versatility of magnetic fields facilitates precise manipulation, due to the flexible use of force and torque, as well as the ability to penetrate non-metallic substrates. Moreover, the low-intensity magnetic fields employed in remote micro-robot control exerts a negligible impact on biological organisms, aligning seamlessly with the stringent requisites of biological systems.

Reducing the size of robotic grippers to the millimeter scale or even smaller while retaining their original functionality is a significant challenge. This not only demands precise fabrication of functional components with tight tolerances but also introduces complexities in actuation parts. Additionally, assembling these components into a functional device becomes exceptionally difficult. The emerging microfabrication technologies like photopolymerization technology, laser cutting, and thin film deposition have provided a promising solution due to their unparalleled precision [5], [6].

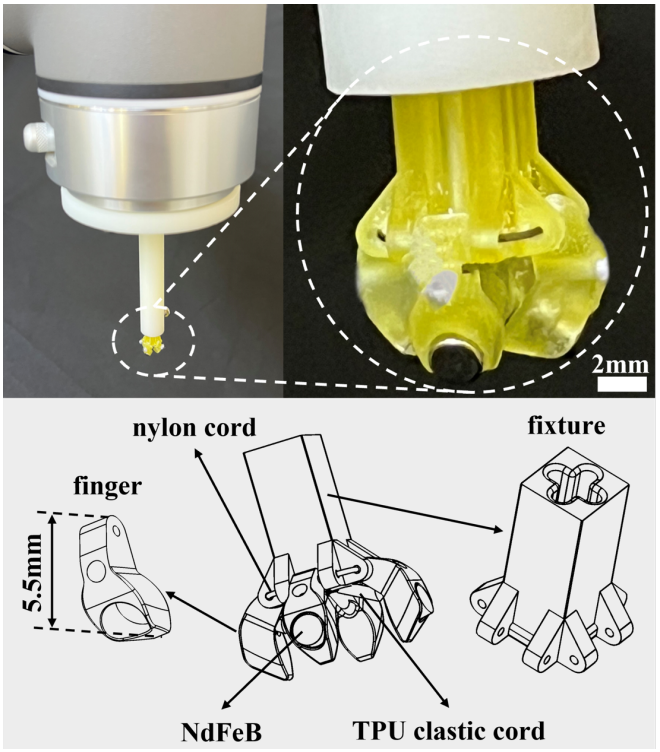

Fig. 1. The miniature magnetic gripper mounted on the UR robotic arm's end-effector. This gripper consists of four fingers and a fixture, with each finger having a maximum length of 5.5mm. A permanent magnet is embedded in each finger and the fingers are connected to the fixture by both nylon and elastic cords. The permanent magnet is used as an internal magnetic actuation unit, the nylon cord acts as a fixation and the elastic cord is responsible for providing the clamping force.

Many researchers have adopted the strategy of integrated processing to directly fabricate miniature grippers. In [7], [8], a micro-gripper capable of intricate pick-and-place tasks within a gradient magnetic field was meticulously fabricated through a multifaceted process, which encompassed techniques such as coating, spin-coating, photolithography, and crosslinking on a silicon wafer. Similarly, a biomimetic jellyfish-inspired soft micro-robot with eight tentacles was created through the casting and laser cutting of magnetic composite materials [9]. In [10], a magnetically elastic rectangular-sheet-shaped soft robot was fabricated using silicone elastomer mixed with magnetic neodymium-iron-

[1] The Institute of Technological Sciences, Wuhan University, Hubei, China
[2] Hubei Luojia Laboratory, Hubei, China
[3] School of Power and Mechanical Engineering, Wuhan University, Hubei,China
[4] Department of Neurosurgery, Renmin Hospital of Wuhan University, Wuhan, Hubei, China
[5] School of Microelectronics, Wuhan University, Hubei, China
[*] Corresponding author.(e-mail: miao.li@whu.edu.cn)

boron microparticles, enabling various motions and gripping actions after magnetization. All of these methods involve conferring controllability by programming magnetization after fabricating the entire structure [11], [12].

To enhance magnetization flexibility, some studies have employed an in-situ magnetization approach, integrating the magnetization process into the printing process itself. For instance, in [13], [14] a method utilizing controlled reorientation of magnetic particles and selective exposure to ultraviolet light was reported, enabling the encoding of magnetic particles into planar materials with arbitrary three-dimensional orientations. However, fabricating miniature multi-fingered manipulators with complex 3D geometries is well beyond the capability of mainstream microfabrication technologies. The necessity to incorporate magnetizable components in the printed materials further restricts the complexity of the printable structures. Consequently, most studies have been limited to producing structures within a 2D plane. While it is possible to transform 2D structures into 3D robotic grippers through careful structural design and ingenious origami methods, significant limitations exist in terms of freedom and functionality [15]–[19].

In light of these considerations, we adopted a component assembly approach. Previous work have demonstrated the feasibility of this method by assembling 3D printed parts and small permanent magnets to create a magnetic gripper with a scissor structure [20], [21]. However, the structure of the planar two-fingered gripper limits its capabilities. In this paper, we introduce a miniature four-fingered magnetic gripper as shown in Fig. 1. The main contributions are as follows:

1) A novel approach was developed to design, manufacture, and assemble the miniature magnetic gripper.

2) A magnetic gripper kinematic model was established by combining physical model and data-driven approach, demonstrating the relationship between the open angle and the external magnetic field.

The reminder of this paper is organized as follows: The fabrication, modeling and analysis of the proposed magnetic gripper are shown in Section II. The experimental results are presented in Section III to demonstrate the effectiveness of this gripper, with a discussion on the limits of the current design, followed by a conclusion in Section IV.

II. MODELING AND ANALYSIS

This section describes in detail the design concept and fabricating process of the proposed miniature magnetic gripper. In order to achieve precise control of the gripper, we modeled and analyzed the function of the gripper under external magnetic field.

A. Design and Fabricating Progress

This study aims to miniaturize macroscopic mechanical grippers and design a millimeter-scale gripper device. Traditional macroscopic mechanical gripers are typically assembled by hydraulic actuators, joints, and mechanical structures. However, scaling down and assembling these components at the microscale presents significant challenges. Therefore, we propose an innovative design approach that utilizes a combination of magnetic and elastic materials instead of hydraulic actuators to control the open-close of the miniaturized gripper, enabling microscale assembly. As illustrated in Fig. 2, the miniature gripper is structured by four fingers and one fixture. Each finger is threaded through the bottom of the fixture with a 0.5mm nylon cord, allowing it to rotate exclusively around the nylon cord. Additionally, each finger is connected to the fixture via a 0.5mm Thermoplastic Polyurethane (TPU) elastic cord with a predetermined pre-stretch, ensuring that the four fingers exert a clamping force in the absence of external forces. To provide magnetic propulsion to the gripper, a miniature cylindrical NdFeB(N35) permanent magnet with a diameter and thickness of 2mm, magnetized along the thickness direction, is embedded on each finger. The four fingers and fixture were 3D-printed with photosensitive resin using the projection micro stereolithography (nanoArch S140, Boston Micro Fabrication, China), ensuring ultra-high precision (10μm) to achive precise assembly. The maximum lengths of the finger in the x, y, and z directions are approximately 5.5mm, 4mm and 3mm, respectively. Each finger is designed with specific features: the upper part has a 0.6mm diameter hole for attachment to the fixture through nylon cord, the middle part features a 0.8mm diameter hole to secure the TPU elastic cord, and the lower section includes a dedicated space to accommodate a small magnet. The fixture is a rectangular prism measuring 4mm in length, 4mm in width, and 10mm in height. Its bottom section is equipped with 8 clamping plates, each with a 1mm thickness, to securely hold the four fingers in place using nylon cord. A 0.6mm diameter hole is positioned at the center of each clamping plate. The top part of the fixture can be utilized to connect with other components, such as a robotic finger, and its size is adjustable to meet specific usage requirements. In the aforementioned assembly process, the connection between the nylon cord and the fingers, as well as the fixture, employs clearance fit. The magnets are securely fixed within the reserved spaces

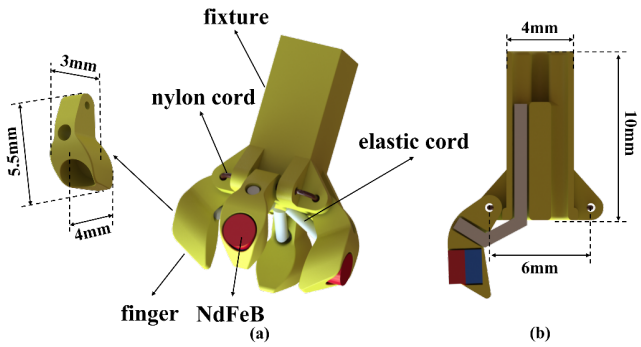

Fig. 2. The design concept and 3D model of the proposed magnetic gripper. (a) The gripper has four fingers and a gripper fixture. Each finger is threaded through the gripper fixture with a nylon cord and a TPU elastic cord. In addition, a NdFeB permanent magnet is embedded in each finger as a drive unit. (b) Profile of the magnetic gripper.

on the fingers using interference fit. The TPU elastic cord is affixed to both the fingers and the fixture at its ends using ethyl cyanoacrylate.

B. Gripper Model and Inner Torque Analysis

The actuation of magnetic gripper relies on forces and torques acting on the embedded magnetic components under external magnetic fields. When a magnetic dipole with a magnetic moment $\mathbf{m} \in \mathbb{R}^3$ is located at a position in free space under an external magnetic field $\mathbf{B} \in \mathbb{R}^3$, the force and torque can be expressed as follows [22]:

$$\begin{cases} \mathbf{F} = (\mathbf{m} \cdot \nabla)\mathbf{B} \\ \mathbf{T} = \mathbf{m} \times \mathbf{B} \end{cases} \tag{1}$$

where $(\mathbf{m} \cdot \nabla)$ is the directional derivative in the direction of $\mathbf{m}$ multiplied by its magnitude. $\mathbf{F} \in \mathbb{R}^3$ and $\mathbf{T} \in \mathbb{R}^3$ are torque and force exerted by the magnetic field.

The magnetic moment $\mathbf{m}$ of a permanent magnet can be calculated as:

$$\mathbf{m} = \iiint_V \mathbf{M} dv = \frac{1}{\mu_0} \mathbf{B}_r V \tag{2}$$

where $\mathbf{M} \in \mathbb{R}^3$ is the magnetization that measures the average magnetic moment density in the magnetic media, $\mu_0 = 4\pi \times 10^{-7}$H/m is the permeability of vacuum and V is the volume of the magnet. For NdFeB, $||\mathbf{B}_r|| = 1200$mT is the residual flux density. Due to the small size of the magnet, the magnetic dipole model can be used to calculate the magnetic field of the magnets [20]. According to the magnetic dipole model, the magnetic field of a magnet is related to its magnetic moment $\mathbf{m}$ and the distance $||\mathbf{r}||$, where $\mathbf{r} \in \mathbb{R}^3$ is a vector from the center of the magnetic dipole to the location where the magnetic field is measured. $\hat{\mathbf{r}}$ is used to express the unit vector of the location vector ($\mathbf{r} = ||\mathbf{r}||\hat{\mathbf{r}}$). The magnetic field $\mathbf{B}_{dipole} \in \mathbb{R}^3$ of the magnetic dipole can be expressed as:

$$\mathbf{B}_{dipole}(\mathbf{r}) = \frac{\mu_0}{4\pi} \left(\frac{3\mathbf{r}\left(\mathbf{m}^\top \mathbf{r}\right)}{\|\mathbf{r}\|^5} - \frac{\mathbf{m}}{\|\mathbf{r}\|^3} \right) \tag{3}$$

The magnetic gripper is a symmetrical structure. In this paper, we consider a situation where the magnetic field exerts symmetric forces on each finger, ensuring that all fingers share the same open angle. Consequently, our analysis will focus solely on the forces and torques acting on finger1. As shown in Fig. 3(a), a local coordinate system has been established with its origin located at the base (center of bottom) of the gripper fixture. The Z-axis coincides with the axis of the fixture. The unit vectors for the four magnetic moments are denoted as $\hat{\mathbf{m}}_1$, $\hat{\mathbf{m}}_2$, $\hat{\mathbf{m}}_3$ and $\hat{\mathbf{m}}_4$, respectively. α, β and θ are defined to represent the open status of the gripper. θ is the open angle, α is determined by the design of the gripper with a value of 24°, while $\beta = \theta - \alpha$, represents the angle between $\hat{\mathbf{m}}_1$ and the Y-axis. a = 3mm is the value of the distance from the origin to the finger junction, $\mathbf{r}_1$ denotes the vector of the magnetic dipole of finger1 to its connection point with a value of b = 3.75mm. In addition, the

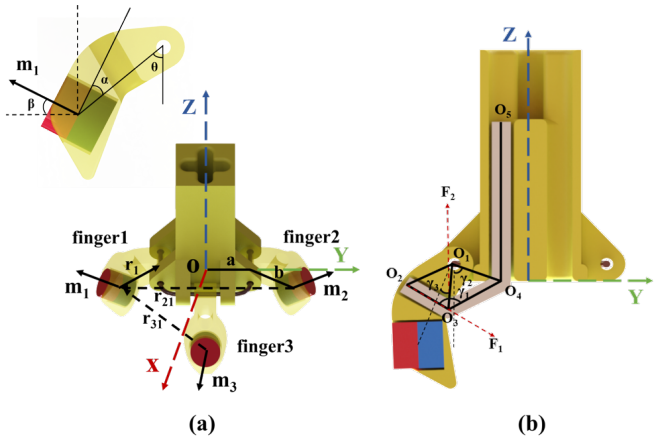

Fig. 3. The local coordinate system for the magnetic gripper. (a) Magnetic field force analysis between the four fingers; (b) Analysis of the force exerted by the elastic cord on finger1.

position vector from the magnetic dipole of finger2 to that of finger1 we denote by $\mathbf{r}_{21}$. The naming rules between the remaining locations follow the above approach. Therefore, the following can be obtained:

$$\begin{cases} \hat{\mathbf{m}}_1 = \begin{bmatrix} 0 & -\cos\beta & \sin\beta \end{bmatrix}^\top \\ \hat{\mathbf{m}}_2 = \begin{bmatrix} 0 & \cos\beta & \sin\beta \end{bmatrix}^\top \\ \hat{\mathbf{m}}_3 = \begin{bmatrix} \cos\beta & 0 & \sin\beta \end{bmatrix}^\top \\ \hat{\mathbf{m}}_4 = \begin{bmatrix} -\cos\beta & 0 & \sin\beta \end{bmatrix}^\top \\ \mathbf{r}_{21} = \begin{bmatrix} 0 & -2(a+b\sin\theta) & 0 \end{bmatrix}^\top \\ \mathbf{r}_{31} = \begin{bmatrix} -(a+b\sin\theta) & -(a+b\sin\theta) & 0 \end{bmatrix}^\top \\ \mathbf{r}_{41} = \begin{bmatrix} a+b\sin\theta & -(a+b\sin\theta) & 0 \end{bmatrix}^\top \\ \mathbf{r}_1 = \begin{bmatrix} 0 & b\sin\theta & b\cos\theta \end{bmatrix}^\top \end{cases} \tag{4}$$

The torque $\mathbf{T}_{21}$, $\mathbf{T}_{31}$ and $\mathbf{T}_{41}$ exerted by the magnetic dipole of other fingers to finger1 can be expressed as:

$$\begin{cases} \mathbf{T}_{21}(\theta) = \mathbf{m}_1 \times \mathbf{B}_2 \\ \mathbf{T}_{31}(\theta) = \mathbf{m}_1 \times \mathbf{B}_3 \\ \mathbf{T}_{41}(\theta) = \mathbf{m}_1 \times \mathbf{B}_4 \end{cases} \tag{5}$$

The torque $\mathbf{T}_{\mathbf{F_{21}}}$, $\mathbf{T}_{\mathbf{F_{31}}}$ and $\mathbf{T}_{\mathbf{F_{41}}}$ generated by forces $\mathbf{F}_{21}$, $\mathbf{F}_{31}$ and $\mathbf{F}_{41}$ can be calculated as follows:

$$\begin{cases} \mathbf{T}_{\mathbf{F}_{21}}(\theta) = \mathbf{r}_1 \times \nabla(\mathbf{m}_1 \cdot \mathbf{B}_2) \\ \mathbf{T}_{\mathbf{F}_{31}}(\theta) = \mathbf{r}_1 \times \nabla(\mathbf{m}_1 \cdot \mathbf{B}_3) \\ \mathbf{T}_{\mathbf{F}_{41}}(\theta) = \mathbf{r}_1 \times \nabla(\mathbf{m}_1 \cdot \mathbf{B}_4) \end{cases} \tag{6}$$

In addition to the magnetic field forces, each finger experiences the forces exerted by the elastic cord. Due to the slender profile of the elastic cord and the significantly larger bending radius compared to its own radius, the elastic cord can be approximated as an idealized thin line. The mechanical model illustrating the relationship between the elastic cord and finger1 is presented in Fig. 3(b). Because the elastic cord is adhered to both ends, one on the finger and the other on the fixture, finger1 primarily experiences the tension at the points $\mathbf{O}_2$ of adhesion and the resultant

force at the bending point $\mathbf{O}_3$. $\mathbf{F}_1$ is directed from point $\mathbf{O}_2$ to $\mathbf{O}_3$ and represents the tension in the elastic rope at point $\mathbf{O}_2$. $\mathbf{F}_2$ is the resultant force of the tension in the elastic rope at point $\mathbf{O}_3$, making an angle $\gamma_1/2$ with respect to the line $\mathbf{O}_2\mathbf{O}_3$. γ_1 is the angle between $\mathbf{O_3O_2}$ and $\mathbf{O_3O_4}$, $\gamma_2 = 60^\circ$ is the angle between $\mathbf{O_1O_4}$ and the Y-axis ,$\gamma_3 = 10^\circ$ is the angle between $\mathbf{O_1O_3}$ and point $\mathbf{O_1}$ to the magnetic moment and $\gamma = 51^\circ$ is the angle between $\mathbf{O_2O_1}$ and $\mathbf{O_2O_3}$. For ease of expression, we denote $\mathbf{O}_2\mathbf{O}_3$ by $\mathbf{L_{23}}$. The rest of the similar expressions follow this rule. k is the elastic constants with a value of 135 of the TPU elastic cord, $||\mathbf{O_2O_3}|| = 2mm$ and $||\mathbf{O_4O_5}|| = 7mm$. $L = 10mm$ represents the original length of the elastic cord. $||\mathbf{O_2O_1}||$ = 2.5mm, $||\mathbf{O_1O_4}||$ = 2mm and $||\mathbf{O_3O_1}||$ = 1.85mm. The total torque $\mathbf{T}_c$ exerted on finger1 from the elastic cord can be calculated as:

$$\begin{aligned}\mathbf{T}_c(\theta) &= \mathbf{T}_{F_1}(\theta) + \mathbf{T}_{F_2}(\theta) \\ &= \mathbf{L_{21}} \times \mathbf{F}_1(\theta) + \mathbf{L_{31}} \times \mathbf{F}_2(\theta)\end{aligned} \tag{7}$$

The torque on finger1 without external magnetic field can be calculated by adding the above torques. Because these torques are produced by the gripper itself, we call it 'inner torque', represented by $\mathbf{T}_{in}$ as:

$$\begin{aligned}\mathbf{T}_{in}(\theta) = \mathbf{T}_{21}(\theta) + \mathbf{T}_{31}(\theta) + \mathbf{T}_{41}(\theta) + \\ \mathbf{T}_{\mathbf{F}_{21}}(\theta) + \mathbf{T}_{\mathbf{F}_{31}}(\theta) + \mathbf{T}_{\mathbf{F}_{41}}(\theta) + \mathbf{T}_c(\theta)\end{aligned} \tag{8}$$

Combined with (3), (4), (5), (6), (7) and (8), the value of the inner torque $T_{in}(\theta)$ around the nylon cord can be calculated as follow:

$$\begin{aligned}T_{in}(\theta) = &-\frac{(1+2\sqrt{2})\|\mathbf{B}_r\|^2 V^2 \sin\beta\cdot\cos\beta}{32\pi\mu_0(a+b\sin\theta)^3} \\ &-\frac{9b\|\mathbf{B}_r\|^2 V^2 \sin\theta\cdot\cos^2\beta}{16\pi\mu_0(a+b\sin\theta)^3} + \frac{15b\|\mathbf{B}_r\|^2 V^2 \sin\theta\cdot\cos^2\beta}{4\pi\mu_0(a+b\sin\theta)^2} \\ &+k\Delta l\cdot L_{21}\cdot\sin\gamma \\ &-k\Delta l\cdot\sqrt{2-2\cdot\cos\gamma_1}\cdot L_{31}\cdot\sin(\theta-\gamma_3)\end{aligned} \tag{9}$$

III. EXPERIMENT AND RESULTS

In this section, calculations and experiments are carried out to verify the accuracy and control reliability of the magnetic gripper.

A. Data-Driven External Magnetic Model

To harness the advantages of high efficiency, stability and compactness, a NdFeB permanent magnet with a 50mm diameter and 30mm thickness, magnetized along the thickness direction, was employed as the control magnet. When applying the magnetic field, it is necessary to keep the axis of the control magnet coincident with that of the gripper fixture. This ensures uniform torque on each finger, thereby maintaining consistency in the magnetic gripper's open-close motion. While symmetrical structures offer computational convenience, the larger size of the control magnet renders the dipole model impractical. Moreover, precisely modeling the magnetic field distribution around a permanent magnet is inherently intricate and challenging, making the calculation of magnetic forces between the control magnet and magnetic grippers a complex task.

To solve the problem, we adopted a data-driven approach to model the relationship between the control magnet and the magnetic gripper. In this paper, we utilized the finite element method within COMSOL [1] to simulate the magnetic torque experienced by the small magnet embedded in the fingers. As illustrated in Fig. 4(a), a series of magnetic torques encountered by the finger as it rotated around the nylon cord were simulated. Fig. 4(b) represents the magnetic flux density between the small magnet in the finger and the control magnet at a certain time in the COMSOL simulation. In the simulations, we calculated the relationship between the open angle and the magnetic torques for a number of cases where the height was increased from 5mm to 40mm with a pitch of 1mm, the open angle was increased from 0° to 90° with a pitch of 1°. In this paper, the height refers to the vertical distance from the base of the magnetic gripper to the surface of control magnet. In total, 35×90=3150 sets of data were obtained, where the ratio used for training and validation is 8:2.

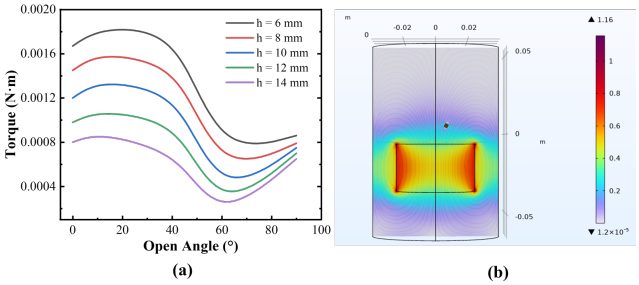

Fig. 4. Simulation results obtained by comsol. (a) The magnetic torque experienced by the finger as it rotates around the axis of the nylon cord when the open angle varies from 0° to 90°, while the base the gripper fixture is at a certain heights from the surface of the control magnet. This figure present the relationship curves between the open angles and the external magnetic torques at six different heights. (b) The magnetic flux density between the small magnet in the finger and the control magnet at a certain time in the COMSOL simulation.

The training data is a set of simulated data $D = \{T_i, \theta_i, h_i\}_{i=1,\ldots,N}$, where T_i, θ_i and h_i denote the moment i in time when the magnetic gripper is at a height and angle relative to the control magnet with values h_i and θ_i respectively, the internal small magnet within the fingers experiences a magnetic torque denoted as T_i. This is a supervised learning task, where the parameters π of a function approximator $F(T, \theta; \pi)$ need to be optimized to accurately map T and θ to corresponding height h:

$$\underset{\theta}{\text{minimize}} \sum_i \ell\left(F\left(T_i, \theta_i; \pi\right), h_i\right) \tag{10}$$

where ℓ denotes the loss function, we employ the form of mean square error here. Given that all the data are low-dimensional, a neural network consisting of three fully connected layers was constructed to train the strategy. The input layer of this network comprises magnetic torque T and angle θ. The first hidden layer of the network transforms

[1]Comsol Multiphysics, Version 6.1, Comsol Group, www.comsol.com.

the input data from two dimensions to 128 dimensions, followed by the second hidden layer further reducing it to 64 dimensions. The final output layer is one-dimensional and is used to predict the height h.

B. Model Validation

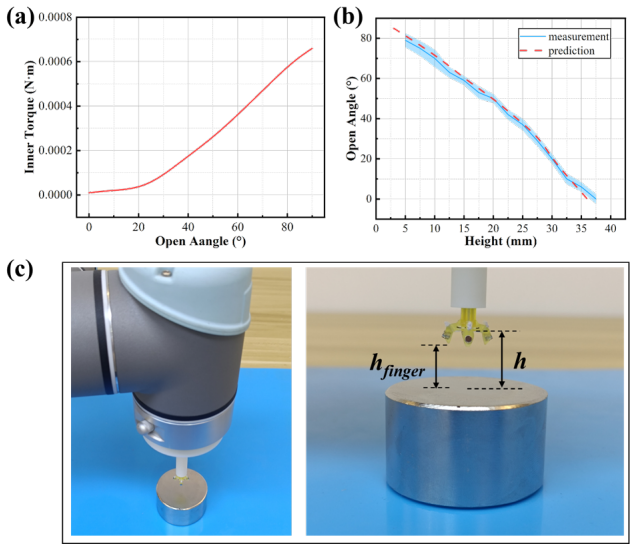

Fig. 5. Verification of the gripper model. (a) The relationship curve between the open angle and the inner torque calculated from the magnetic gripper model. (b) Blue area: Plot of gripper open angle versus height measured by 5 repeated experiments; Red dashed line: The relationship curve between the open angle and height fitted by the magnetic gripper model. (c) The experiment setup for measuring the relationship between open angle and height.

According to (9), the relationship between the open angle and the inner torque shown in Fig. 5(a) can be obtained. Based on this, a series of inner torques and open angles were input into the well-trained neural network, and the corresponding height at each moment was predicted. The relationship between the open angle and height, as depicted by the red dashed line in Fig. 5(b), can be fitted accordingly.

As shown in Fig. 5(c), the magnetic gripper was securely attached to the end-effector of the robotic finger (collaborative robot UR5e, UniversalRobots, Denmark) using a customized flange. To get the experimental data, first adjust the base of magnetic gripper to 40mm away from the control magnet, then slowly descend to 5mm. The distance from the gripper base to the surface of the controlled magnet is indicated by h in the figure. The open angle of the gripper in the entire descent process is determined by measuring the bottom of the fingers from the control magnet, as indicated by h_{finger} in the figure, in conjunction with calculations based on the gripper's structure design. The blue area in Fig. 5(b), which calculated by five repeated experiments, shows the relationship between the actual open angle and height. Further calculations show that the average error between the experimental measured open angles and the predicted results of the magnetic gripper model is 2.31°.

C. Precision Grasp Experiments

The ability to precisely control the open-close of a gripper is important for delicate manipulation. For this reason, we designed the experiments shown in Fig. 6. We first designed a fragile cylinder part with a layer of 5mm outer diameter, 0.1mm thickness and 6mm height shell in the upper part. The results show that when the open angle of the gripper is accurately controlled according to the model, the part can remain complete. During the precision control process, we first measured the dimensions of the grasped object, calculated the required open angle of the gripper, and then place the control magnet at the corresponding distance below. As the gripper move to the gripping position, the control magnet is slowly lowered. At this time, the grippers will gradually close around the object under the influence of internal torque, preventing any damage. When attempting to grasp a fragile object with an arbitrary open angle, a large open angle may potentially cause the gripper to close rapidly when the magnetic field quickly diminishes, which can result in damage to the object. The above experiments also demonstrate the necessity of an accurate control model.

D. Sensitivity Testing Experiments

In order to verify the sensitivity of this magnetic gripper to the magnetic field, we designed an experiment shown in Fig. 7. Specifically, we tested the change in the open angle of the magnetic gripper as it moved from 40 mm to 5 mm above the control magnet in 1, 2, and 4 seconds, respectively. The results show that despite different speeds the gripper approaching the control magnet, there is little difference in the open angle at similar positions, indicating the excellent sensitivity of the magnetic gripper to the magnetic field.

E. Tissue Grasping Experiments

In practical applications, this magnetic gripper can be used for the removal of gastric polyp tissue. To simulate this situation we designed the following experiments. First, we simulated the force between biological tissues with a sponge stuck to a transparent tape as shown in Fig. 8(a). Further, a piece of grape was excised as a grasping object to simulate the texture of biological tissues as shown in Fig. 8(b). The results of simulation experiments show that the magnetic gripper fulfills these task successfully, demonstrating its potential in real applications.

Although the above experiments have shown some excellent performance of our designed magnetic gripper, there are still some problems to be solved. Firstly, the dimensions of the gripper still need to be further reduced in order to expand its practical applications. In addition to optimizing the structure, the use of embedded magnetic particles instead of permanent magnets could be considered in the future, which could significantly reduce the size of gripper. Secondly, in terms of control the permanent magnet can be assembled to the end-effector of another robotic arm. In the future we will build a closed-loop magnetic control system based on dual-arm by combining the feedback from visual and tactile sensors to make the operation more flexible.

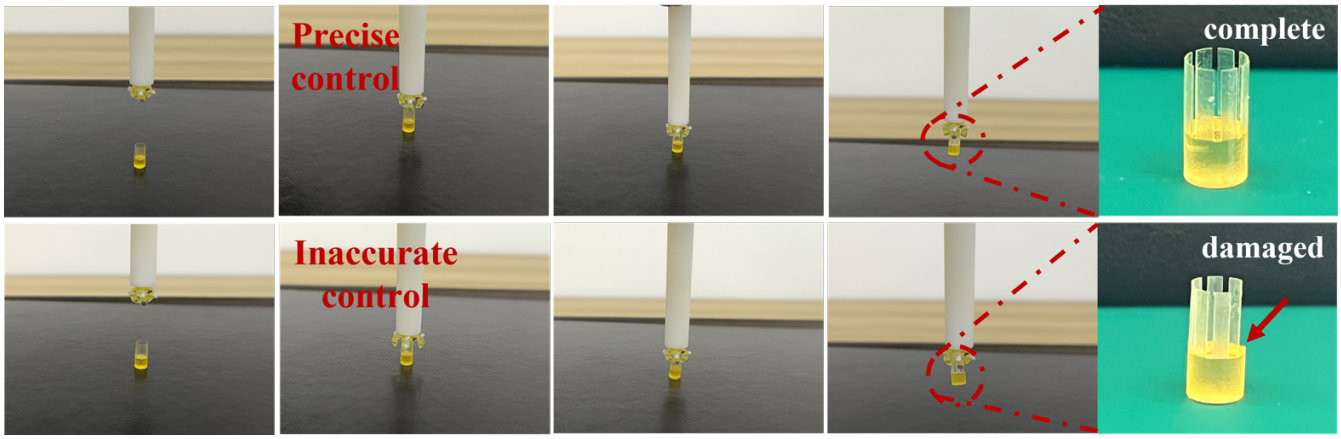

Fig. 6. The precision grasp experiments.

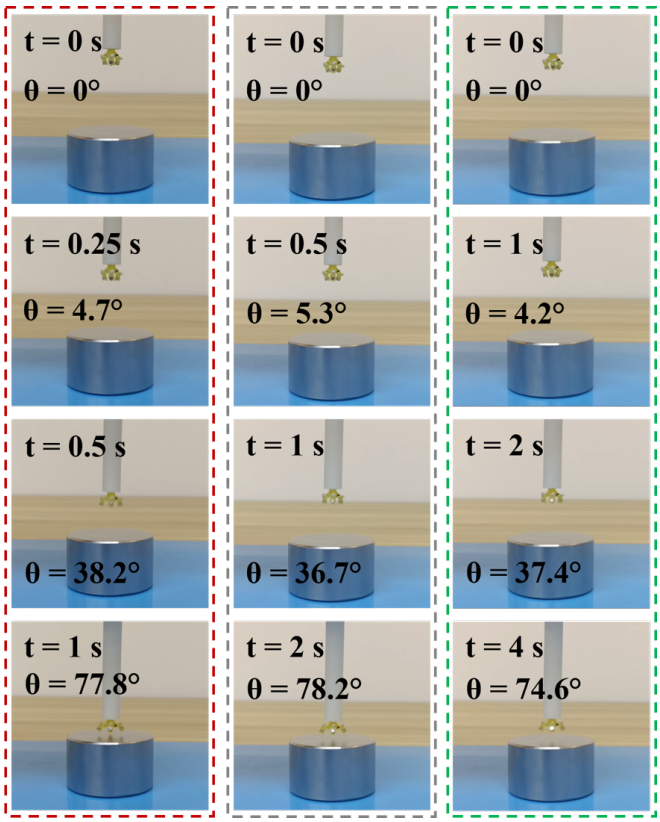

Fig. 7. The sensitivity testing experiments.

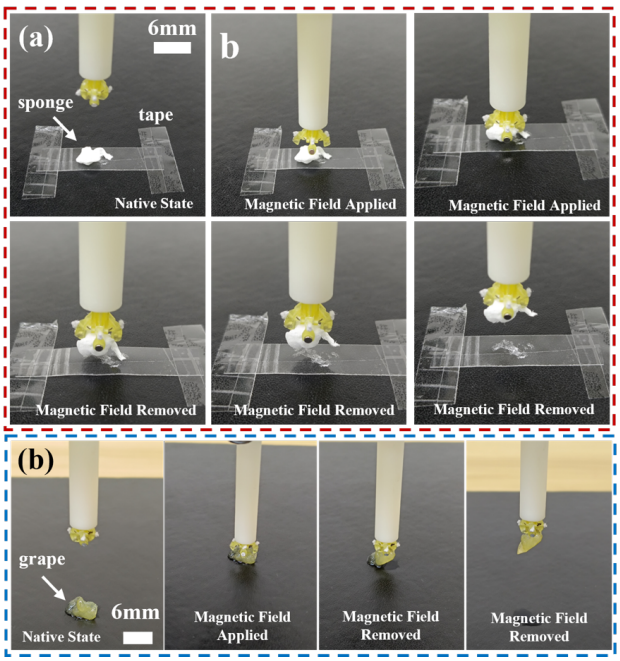

Fig. 8. The simulated tissue grasping experiments. (a) Grasp a sponge that is stuck to the clear adhesive. (b) Grasp a piece of grape pulp.

IV. CONCLUSION

This paper introduces an innovative miniature magnetic gripper designed for MIS applications. The construction design, assembly method and functionality of the magnetic gripper are comprehensively detailed. Through physical analysis, we established an internal torque model for the magnetic gripper. Combined with the external magnetic torque model obtained from the neural network, we created a kinematic control model for the gripper. The open-close experiments demonstrate the accuracy of the gripper model and its sensitivity to the magnetic field, where the average error between the experimentally measured open angles and the results predicted by the model is 2.31°. The grasping experiments demonstrate the necessity of the magnetic gripper model and the potential of the gripper for future applications in MIS.

ACKNOWLEDGMENT

This work was supported by the Fundamental Research Funds for the Central Universities under the grant agreement number 2042023kf0110, Suzhou Key Industry Technology Innovation Project under the grant agreement number SYG202121 and The Interdisciplinary Innovative Talents Foundation from Renmin Hospital of Wuhan University under the grant agreement number of JCRCYR-2022-002.

REFERENCES

[1] M. Leveziel, W. Haouas, G. J. Laurent, M. Gauthier, and R. Dahmouche, "Migribot: A miniature parallel robot with integrated gripping for high-throughput micromanipulation," *Science Robotics*, vol. 7, no. 69, p. eabn4292, 2022.

[2] C. Forbrigger, A. Lim, O. Onaizah, S. Salmanipour, T. Looi, J. Drake, and E. D. Diller, "Cable-less, magnetically driven forceps for minimally invasive surgery," *IEEE Robotics and Automation Letters*, vol. 4, no. 2, pp. 1202–1207, 2019.

[3] H.-J. Chung, A. M. Parsons, and L. Zheng, "Magnetically controlled soft robotics utilizing elastomers and gels in actuation: A review," *Advanced Intelligent Systems*, vol. 3, no. 3, p. 2000186, 2021.

[4] T. Xu, J. Zhang, M. Salehizadeh, O. Onaizah, and E. Diller, "Millimeter-scale flexible robots with programmable three-dimensional magnetization and motions," *Science Robotics*, vol. 4, no. 29, p. eaav4494, 2019.

[5] F. Wang, C. Liang, Y. Tian, X. Zhao, and D. Zhang, "Design and control of a compliant microgripper with a large amplification ratio for high-speed micro manipulation," *IEEE/ASME Transactions on Mechatronics*, vol. 21, no. 3, pp. 1262–1271, 2016.

[6] G. Shao, H. O. T. Ware, J. Huang, R. Hai, L. Li, and C. Sun, "3d printed magnetically-actuating micro-gripper operates in air and water," *Additive Manufacturing*, vol. 38, p. 101834, 2021.

[7] F. Ongaro, C. Yoon, F. Van Den Brink, M. Abayazid, S. H. Oh, D. H. Gracias, and S. Misra, "Control of untethered soft grippers for pick-and-place tasks," in *2016 6th IEEE International Conference on Biomedical Robotics and Biomechatronics (BioRob)*. IEEE, 2016, pp. 299–304.

[8] S. Scheggi, K. K. T. Chandrasekar, C. Yoon, B. Sawaryn, G. Van De Steeg, D. H. Gracias, and S. Misra, "Magnetic motion control and planning of untethered soft grippers using ultrasound image feedback," in *2017 IEEE International Conference on Robotics and Automation (ICRA)*. IEEE, 2017, pp. 6156–6161.

[9] Z. Ren, T. Wang, W. Hu, and M. Sitti, "A magnetically-actuated untethered jellyfish-inspired soft milliswimmer." in *Robotics: Science and Systems*, 2019, pp. 22–26.

[10] W. Hu, G. Z. Lum, M. Mastrangeli, and M. Sitti, "Small-scale soft-bodied robot with multimodal locomotion," *Nature*, vol. 554, no. 7690, pp. 81–85, 2018.

[11] V. K. Venkiteswaran, L. F. P. Samaniego, J. Sikorski, and S. Misra, "Bio-inspired terrestrial motion of magnetic soft millirobots," *IEEE Robotics and automation letters*, vol. 4, no. 2, pp. 1753–1759, 2019.

[12] J. Kim, S. E. Chung, S.-E. Choi, H. Lee, J. Kim, and S. Kwon, "Programming magnetic anisotropy in polymeric microactuators," *Nature materials*, vol. 10, no. 10, pp. 747–752, 2011.

[13] Z. Wang, Y. Wu, D. Wu, and Z. Hai, "3d printing of magnetically actuated miniature soft robots," in *2021 IEEE 16th International Conference on Nano/Micro Engineered and Molecular Systems (NEMS)*. IEEE, 2021, pp. 804–808.

[14] Y. Kim, H. Yuk, R. Zhao, S. A. Chester, and X. Zhao, "Printing ferromagnetic domains for untethered fast-transforming soft materials," *Nature*, vol. 558, no. 7709, pp. 274–279, 2018.

[15] X. Qian, Y. Zhao, Y. Alsaid, X. Wang, M. Hua, T. Galy, H. Gopalakrishna, Y. Yang, J. Cui, N. Liu, *et al.*, "Artificial phototropism for omnidirectional tracking and harvesting of light," *Nature nanotechnology*, vol. 14, no. 11, pp. 1048–1055, 2019.

[16] Z. Ding, C. Yuan, X. Peng, T. Wang, H. J. Qi, and M. L. Dunn, "Direct 4d printing via active composite materials," *Science advances*, vol. 3, no. 4, p. e1602890, 2017.

[17] O. M. Wani, H. Zeng, and A. Priimagi, "A light-driven artificial flytrap," *Nature communications*, vol. 8, no. 1, p. 15546, 2017.

[18] Y. Dong, J. Wang, X. Guo, S. Yang, M. O. Ozen, P. Chen, X. Liu, W. Du, F. Xiao, U. Demirci, *et al.*, "Multi-stimuli-responsive programmable biomimetic actuator," *Nature communications*, vol. 10, no. 1, p. 4087, 2019.

[19] J. W. Boley, W. M. Van Rees, C. Lissandrello, M. N. Horenstein, R. L. Truby, A. Kotikian, J. A. Lewis, and L. Mahadevan, "Shape-shifting structured lattices via multimaterial 4d printing," *Proceedings of the National Academy of Sciences*, vol. 116, no. 42, pp. 20 856–20 862, 2019.

[20] Y. Mao, S. Yuan, S. Song, and M. Q.-H. Meng, "Design of a magnetically-driven untethered micro-gripper for drug delivery," in *2019 IEEE International Conference on Robotics and Biomimetics (ROBIO)*. IEEE, 2019, pp. 1501–1507.

[21] Y. Mao, S. Yuan, J. Wang, J. Zhang, and S. Song, "Modeling and control of an untethered magnetic gripper," in *2021 IEEE International Conference on Robotics and Automation (ICRA)*. IEEE, 2021, pp. 7274–7280.

[22] Y. Kim and X. Zhao, "Magnetic soft materials and robots," *Chemical reviews*, vol. 122, no. 5, pp. 5317–5364, 2022.